

# Picturing the Transition-State Region and Understanding Vibrational Enhancement for the $\text{Cl} + \text{CH}_4 \rightarrow \text{HCl} + \text{CH}_3$ Reaction

William R. Simpson, T. Peter Rakitzis, S. Alex Kandel, Topaz Lev-On, and Richard N. Zare\*

Department of Chemistry, Stanford University, Stanford, California 94305

Received: September 7, 1995; In Final Form: November 27, 1995<sup>⊗</sup>

Comparison of state-to-state differential cross sections for methane in the ground vibrational state to methane with one quantum of asymmetric stretch excitation probes the effect of C–H stretch excitation on the reaction of atomic chlorine with methane. We previously reported state-to-state differential cross sections and HCl product state population distributions for the vibrationally excited reaction. Here we report analogous measurements of the reaction for methane in the vibrational ground state. Photolysis of molecular chlorine produces chlorine atoms that react with methane molecules at 0.16 eV collision energy. Calibrated resonance-enhanced multiphoton ionization (REMPI) determines the product state distributions, and the core-extraction technique measures the angular scattering distribution. The product  $\text{HCl}(v=0)$  is formed with a cold rotational-state distribution and is strongly back scattered. The product state and angular scattering distributions for the ground-state reaction are consistent with a line-of-centers model in which the cone of acceptance is only narrowly open. The rotational-state distributions and comparisons to thermal rate data indicate that the C–H–Cl angle must be constrained in the transition-state region. One quantum of C–H asymmetric stretch vibrational excitation enhances the rate of reaction at a collision energy of 0.16 eV by a factor of  $30 \pm 15$  ( $\pm 2\sigma$ ). The behavior of the ground-state reaction is in marked contrast to our earlier results for the reaction of chlorine atoms with C–H stretch-excited methane, for which the state-to-state angular scattering distributions were consistent with a widely open cone of acceptance. By using the approximation that hard-sphere scattering describes the relation between impact parameter and scattering angle, we can transform the measured state-to-state differential cross section into the distribution of impact parameters that lead to reaction, which forms what we call a *b* map. This *b* map pictorially shows that the ground-state reaction occurs only for head-on collisions (with small impact parameters), whereas C–H stretch vibrational excitation allows reactivity to spread to the periphery of the methane molecule. The data indicate that the mechanism of vibrational enhancement is opening of the cone of acceptance and lessening the necessity for collinearity of the C–H–Cl angle in the transition-state region.

## 1. Introduction

One of the goals in understanding bimolecular chemical reactions on a microscopic level is to visualize the intimate contact between reactants that lead to products.<sup>1</sup> Direct methods involving probes on the femtosecond time scale are frustrated by the challenge of setting the clock for a true bimolecular reaction. Furthermore, problems exist in interpreting the spectroscopic signature of reactants in close proximity in terms of the behavior on a single potential energy surface. Indirect methods are also generally unsatisfactory because of the difficulty in relating asymptotic scattering properties to the behavior in the transition-state region. For some extremely simple systems, scattering calculations employing reliable potential energy surfaces hold much promise for constructing pictures of how reactions occur, especially when supported by accurate experimental measurements that lend credence to the approximations made in the calculations. Our approach is purely experimental and relies on measuring enough attributes of the reactive scattering process to enable us to infer features of the transition-state structure. Our procedure relies on the ability to obtain state-to-state angular scattering distributions of the products that can be converted, under some assumptions, to the distribution of reactive distances of closest approach of the reagents that result in reaction of a specific type. Particularly informative are comparisons of the nature of the target when a reagent is or is not vibrationally excited. This comparison is

beneficial because vibrational motion is on the time scale of atom transfer, and a direct reaction can be considered a form of vibration of the reagents during intimate contact. Such comparisons help us develop a dynamic picture of the transition-state region.

This paper presents such a treatment for the elementary reaction of a chlorine atom with a methane molecule to form hydrogen chloride and a methyl radical, which is the first step in the thermal or photolytic chlorination of methane. This process often is the first example of a chemical reaction presented in a beginning course on organic chemistry.<sup>2</sup> We investigate reaction of atomic chlorine with normal methane



and with perdeuterated methane



Both are referred to as the ground-state reaction. Investigation of the vibrationally excited reaction



has been described previously.<sup>3–5</sup> The ground-state reaction is endothermic;  $\Delta H = 1.72$  kcal/mol ( $600 \text{ cm}^{-1}$ ;  $0.075 \text{ eV}$ ).<sup>6</sup> It has been investigated via temperature-dependent rate measurements, which showed the reaction to be activated with a barrier of  $2.7$  kcal/mol ( $940 \text{ cm}^{-1}$ ,  $0.115 \text{ eV}$ )<sup>6</sup> based on a fit to

<sup>⊗</sup> Abstract published in *Advance ACS Abstracts*, April 1, 1996.

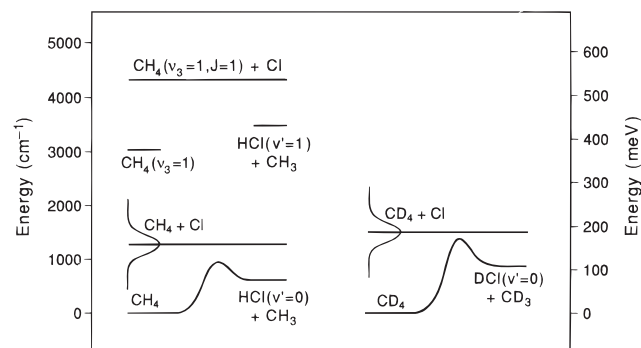


**Figure 1.** Energetics of the reaction of atomic chlorine with methane. The left side of the figure shows the reaction  $\text{Cl}(^2\text{P}_{3/2}) + \text{CH}_4$ , while the right side shows the reaction  $\text{Cl}(^2\text{P}_{3/2}) + \text{CD}_4$ . The zero of energy is set by the energy of the separated reagents. On both sides, the collisional energy spread is represented by the Gaussian distribution that would result from a beam translational temperature of 15 K as calculated from the formulas of van der Zande *et al.*<sup>34</sup> In addition to the ground-state reaction  $\text{Cl}(^2\text{P}_{3/2}) + \text{CH}_4$ , the total energy of the vibrationally excited reaction,  $\text{Cl}(^2\text{P}_{3/2}) + \text{CH}_4(\nu_3=1)$ , is shown for comparison. The change in reaction endothermicity upon deuteration is calculated by application of zero-point energy change (harmonic approximation) on deuteration using published vibrational frequencies. The transition-state energy of the reaction  $\text{Cl}(^2\text{P}_{3/2}) + \text{CD}_4$  is calculated by assuming no zero-point energy for the transferring hydrogen or deuterium atom at the transition state.

Arrhenius behavior over the range 200–300 K. The preexponential factor of the Arrhenius fit is  $A = 9.6 \times 10^{-12} \text{ cm}^3 \text{ molecule}^{-1} \text{ s}^{-1}$ .<sup>6</sup> Figure 1 shows the energetics of this reaction. High-level quantum mechanical calculations of the saddle point energy and geometry were carried out by Truong *et al.*<sup>7</sup> and Dobbs and Dixon.<sup>8</sup> Truong *et al.* found a zero-point-energy corrected barrier of approximately 3.5 kcal/mol (1220  $\text{cm}^{-1}$ ), which is on the high end of the experimentally measured activation energy range. The discrepancy between the calculated and experimental barriers could arise from quantum-mechanical tunneling, which may also be indicated by the deviations from Arrhenius behavior noted in the rate data.<sup>6</sup> These calculations also indicated that the transition state was collinear along the Cl–H–C axis and has a “late” barrier. While the term late barrier is usually reserved for highly endothermic reactions, where the transition state has a productlike geometry, we use the term for this nearly thermoneutral reaction to reflect the calculated productlike geometry of the transition state. Truong *et al.*<sup>7</sup> calculate at the MP-SAC2 level of theory a transition state with 27% stretching of the H–C bond (compared to a H–C bond in isolated methane) and 12% stretching of the H–Cl bond (compared to the H–Cl length in isolated HCl). The greater elongation of the breaking H–C bond than the elongation of the forming H–Cl bond indicates a late transition state. Similarly, Dobbs and Dixon<sup>8</sup> calculate 33% and 8% stretching of the H–C and H–Cl bonds, respectively, at the MP2 level of theory. Wang, Ben-Nun, and Levine<sup>9</sup> have made a classical trajectory calculation of the vibrationally excited reaction using model potential energy surfaces. Duncan and Truong<sup>10</sup> have calculated *ab initio* thermal and vibrational-state selected rates for the Cl + CH<sub>4</sub> reaction. Their results predict that excitation of the CH<sub>4</sub> symmetric stretching mode significantly increases the hydrogen atom abstraction rate.

After a brief description of the experimental setup, we present the HCl product internal-state distribution and the degree of enhancement of this reaction by C–H vibrational excitation of the methane reagent. We also display the state-resolved angular distribution for the ground-state reaction. An approximate picture of the reactivity of the methane target is produced through a simple inversion based on hard-sphere scattering behavior. Marked differences are apparent in the behavior of

vibrationally excited and unexcited methane from which a consistent model can be developed for the vibrational enhancement of this reaction.

## 2. Experimental Section

Most methods used in this study have been described elsewhere.<sup>4,5</sup> Briefly, molecular chlorine, methane, and helium buffer gas premixed in a Teflon-lined tank are expanded from 380 Torr into a vacuum chamber through a pulsed nozzle. Chlorine atoms are produced by photolysis of Cl<sub>2</sub> at 355 nm by frequency tripling a Nd<sup>3+</sup>:YAG laser. Photolysis of molecular chlorine at this wavelength produces >98% ground-state chlorine atoms ( $\text{Cl}(^2\text{P}_{3/2})$ ) that carry 1290  $\text{cm}^{-1}$  of energy in the collision frame with CH<sub>4</sub>. The cooling caused by the jet expansion limits the thermal motions of the molecular chlorine precursors and the methane target molecules, decreasing the thermal broadening of the collision energy distribution. After a short delay (70–170 ns) to allow for reactive product buildup, HCl products are detected by (2 + 1) REMPI, which selectively ionizes single rovibrational states of this product. A linear time-of-flight mass spectrometer detects these product ions. We used REMPI excitation wavelength scans with detection of total H<sup>35</sup>Cl<sup>+</sup> ion current to determine product population state distributions after correction for linestrength and spectroscopic perturbations.

The method of core extraction measures three-dimensional projections of the velocity distribution of the reactive product using a time-of-flight mass spectrometer equipped with a mask to reject off-axis scattered products. This three-dimensional projection is then converted to a state-to-state differential cross section via simple transformations.<sup>11</sup> These transformations are based on a photoinitiated scheme in which the laboratory speed of the center of mass of the reacting system and the speed of the product in the center-of-mass frame are known. These two vectors add to give the laboratory speed of the reactive product; therefore, a measurement of this third side of the scattering triangle determines all angles (including the scattering angle) uniquely. Using this correspondence between the scattering angle and the product laboratory speed, we convert the measured speed distribution to a state-to-state differential cross section (For more details on the method, see ref 11). A growing number of groups are using this method,<sup>11–16</sup> which we refer to as the *photoloc* method,<sup>16</sup> an acronym that stands for photoinitiated reaction determining the differential cross section by the law of cosines.

## 3. Results

**3.1. Rotational-State Distributions.** To investigate the rovibrational distribution from the ground-state reaction, we performed photolysis subtraction. The photolysis laser was operated at half the repetition rate of the probe laser so that the signals from every other probe laser shot could be subtracted to obtain the change in signal caused by the photolysis laser. Because Cl atoms created by the photolysis laser are required for reactive signal, this photolysis difference provides reactive signal while it rejects probe-laser-induced backgrounds. This subtraction procedure was used in the measurement of REMPI wavelength excitation spectra for the ground-state reaction. The REMPI spectra were recorded on the HCl F–X (0,0) band in which  $m/z = 36$  (H<sup>35</sup>Cl<sup>+</sup>) is detected. As shown in Figure 1, only vibrational ground-state HCl products are possible. The REMPI spectra were converted to populations using previously published correction factors.<sup>5</sup> Figure 2a shows a plot of the HCl( $\nu=0, J$ ) product rotational-state populations from the Cl + CH<sub>4</sub> reaction. Significant background HCl( $\nu=0, J$ ) from pre-reaction of chlorine with contaminant in our mixing tank is

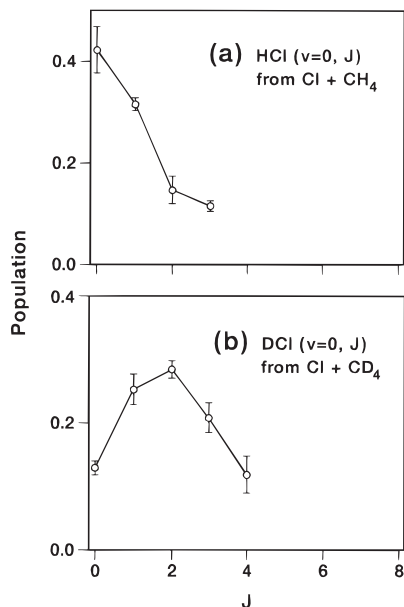


**Figure 2.** Plots of state distributions from the reactions of atomic chlorine with ground-state  $\text{CH}_4$  and  $\text{CD}_4$ . Panel a shows the result for the  $\text{HCl}(v=0, J)$  product of the reaction  $\text{Cl} + \text{CH}_4$ . Panel b shows the result for the  $\text{DCl}(v=0, J)$  product of the reaction  $\text{Cl} + \text{CD}_4$ . Error bars represent 95% confidence limits (based only on statistics).

observed on all product states. Although the subtraction procedure results in the reactive product-state distribution, the background signals make the experiment more difficult and increase the possibility of systematic error; therefore, the reaction  $\text{Cl} + \text{CD}_4$  is investigated to provide a ground-state reaction with essentially no background. We recorded REMPI spectra on the  $\text{DCl F-X}(0,0)$  band in which  $m/z = 37$  ( $\text{D}^{35}\text{Cl}^+$ ) is detected. Line intensities from these spectra were converted to populations through comparison to calibration REMPI spectra performed on thermal  $\text{DCl}$  samples. Figure 2b shows a plot of the  $\text{DCl}(v=0, J)$  product rotational-state populations from the  $\text{Cl} + \text{CD}_4$  reaction. Both rotational-state distributions are very cold; the  $\text{HCl}$  from  $\text{Cl} + \text{CH}_4$  contains  $31 \pm 5 \text{ cm}^{-1}$  ( $\pm 2\sigma$  error bar) average rotational energy, and the  $\text{DCl}$  from  $\text{Cl} + \text{CD}_4$  has  $38 \pm 7 \text{ cm}^{-1}$  average rotational energy.

**Vibrational Enhancement Factor.** A combination of IR and “time-jump” subtraction was used to measure  $\text{Cl} + \text{CH}_4$  vibrational enhancement. The IR subtraction procedure involves recording the difference between signals for which the IR laser excites methane and signals for which the IR laser is blocked. IR subtraction was used to measure the reaction of vibrationally excited methane. The time-jump subtraction procedure relies on the fact that the product of the reaction builds in time between the photolysis laser pulse and the probe laser pulse. Therefore, subtraction of signals with a short photolysis–probe delay ( $\approx 20$  ns) from those with a long photolysis–probe delay (70–170 ns) measures the reactive signal. We discuss IR and time-jump subtraction procedures quantitatively to make completely clear the subtraction procedures used to measure the vibrational enhancement factor. Using both subtraction procedures results in four signals; we call these signals  $G_s$ ,  $G_l$ ,  $I_s$ , and  $I_l$ . The symbol  $G$  stands for ground-state signal (IR excitation blocked) and  $I$  stands for IR-excited signal (with IR excitation). The subscripts  $s$  and  $l$  stand for short and long photolysis–probe time delays, respectively. Without IR excitation and at short time delay,

$$G_s = B + gt_s \quad (3)$$

where  $B$  represents all background contributions that do not depend on photolysis–probe delay,  $g$  is the ground-state rate,

and  $t_s$  is the short time delay. We initially assume that the product builds linearly in time, but this presumption is generalized subsequently. At long time delay,

$$G_l = B + gt_l \quad (4)$$

where  $t_l$  is the long time delay. Time-jump subtraction of these signals results in

$$G_l - G_s = g(t_l - t_s) \quad (5)$$

which removes the background and yields the rate,  $g$ , of the ground-state reaction.

The assumption that the product concentrations grow linearly in time is unnecessary; the only requirement is that each product’s time dependence is equal. For example, flyout of reagent chlorine atoms or product  $\text{HCl}$  molecules does not affect the product rotational-state distribution as long as each product state does not fly out differently. For this reason, the small amount of flyout corrected for in the speed distribution analysis (as discussed later) is not needed to correct the population distributions.

We repeat this subtraction procedure with IR excitation. Because only a fraction of the methane molecules are vibrationally excited, the IR signal has both ground-state and vibrationally excited contributions. Therefore, at some time,  $t$ , after initiation

$$I = B + fvt + (1 - f)gt \quad (6)$$

where  $f$  is the fraction of molecules vibrationally excited and  $v$  is the vibrationally excited reaction rate. Consider the IR difference

$$\begin{aligned} I - G &= fvt + (1 - f)gt - gt \\ &= f(v - g)t \end{aligned} \quad (7)$$

Note that the fraction excited only changes the total signal intensity; therefore, IR subtraction reveals the difference between the total ground-state and total excited-state reactions. Thus, state distributions recorded with IR subtraction at fixed excitation fraction reflect the difference of the reactions of the vibrationally excited and ground-state methane.

For determination of the vibrational enhancement factor, it is most convenient to use the difference:

$$(I_l - G_l) - (I_s - G_s) = f(v - g)(t_l - t_s) \quad (8)$$

Solving for the vibrationally induced product,

$$v(t_l - t_s) = \left( \frac{[(I_l - G_l) - (I_s - G_s)]}{f} + g(t_l - t_s) \right) \quad (9)$$

Division by eq 5 results in the vibrational enhancement factor

$$\frac{v}{g} = \left( \frac{(I_l - G_l) - (I_s - G_s)}{f(G_l - G_s)} + 1 \right) \quad (10)$$

Use of this procedure with REMPI via the  $\text{F-X}(0,0)$   $\text{R}(3)$  line and  $\text{H}^{35}\text{Cl}^+$  detection (integrated over the time profile) results in the vibrational enhancement for  $\text{HCl}(v=0, J=3)$ . The signal ratio between the IR-subtracted time-jump difference (eq 8) and the ground-state-reaction time-jump difference (eq 5) was determined to be  $8 \pm 4$  for  $\text{HCl}(v=0, J=3)$ .

The vibrational excitation probability was estimated by measuring the dependence of the vibrationally excited signal on the IR laser power. This power dependence was significantly

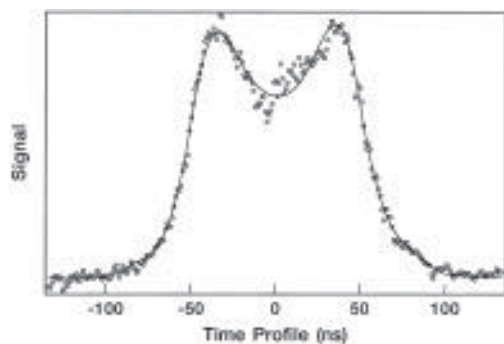


**Figure 3.** Coadded core-extracted time profile for detection of DCI( $\nu=0, J=0$ ) on S(0) of F-X (0,0) band from the reaction of Cl with ground-state CD<sub>4</sub>. The symbols show the experimental data, and the line shows the fit.

less than linear, indicating saturation of the Q-branch excitation line; therefore, a significant number of molecules in this spectral feature are excited. The infrared laser excites Q(1), Q(2), and Q(3) under its  $\sim 1-2 \text{ cm}^{-1}$  bandwidth. We estimate that more than half of the CH<sub>4</sub> molecules populate these three rotational states. Taking these two pieces of data together, we estimate  $f = 0.25$  under the present experimental conditions. Therefore, the state-resolved vibrational enhancement factor for HCl( $\nu=0, J=3$ ) is  $33 \pm 16$ . To arrive at the total (summed over all product rovibrational states) enhancement (referred to as  $\sigma_v/\sigma_g$ ), we scale the state-resolved enhancement  $v/g$  by the relative populations of HCl( $\nu=0, J=3$ ) for both reactions. This procedure results in a total enhancement ratio of

$$\sigma_v/\sigma_g = 30 \pm 15 (\pm 2\sigma) \quad (11)$$

The error in the measurement is purely statistical and is caused primarily by the subtraction error that comes from removal of HCl( $\nu=0, J=3$ ) background signals arising from prereaction in the tank. The vibrational enhancement factor has a magnitude expected for an endothermic reaction with a late barrier. In such systems, vibration is expected to be more effective than translation in promoting reaction.<sup>17,18</sup>

**3.2. Angular Scattering Distributions.** The presence or absence of a photolysis laser pulse changes the background signals at mass 35 and 37, which interferes with measurement of product velocity distributions. We believe this background change is caused by probe-laser-induced nonresonant dissociative ionization of Cl<sub>2</sub>, which results in <sup>35</sup>Cl<sup>+</sup> and <sup>37</sup>Cl<sup>+</sup>. The amount of this background depends on the presence of the photolysis laser because the concentration of Cl<sub>2</sub> is depleted by the photolysis laser pulse. This change has no effect on mass-resolved REMPI spectra used in the determination of rotational-state distributions and vibrational enhancement factors, but measurements of speed distributions with core extraction are distorted. For this reason, speed distribution measurements used the time-jump subtraction procedure. Time-jump subtraction measures only signals that increase with photolysis-probe time delay; therefore, it has advantages over simple photolysis on-off subtraction in that it eliminates background signals from both the photolysis and probe lasers as well as signal from any cluster reactions. We have checked for cluster reactions and found no evidence of them under the current experimental conditions. Speed distributions were measured with core extraction using time-jump subtraction.

Figure 3 plots the DCI( $\nu=0, J=0$ ) core-extracted time profile recorded at 62 V/cm extraction field from the Cl + CD<sub>4</sub> reaction. Results for the Cl + CD<sub>4</sub> reaction are shown because the background is lower than that for the Cl + CH<sub>4</sub> reaction. The data shown are the coaddition of polarized photolysis time profiles with the weighted summation  $I_{\text{par}} + 2I_{\text{perp}}$ .  $I_{\text{par}}$

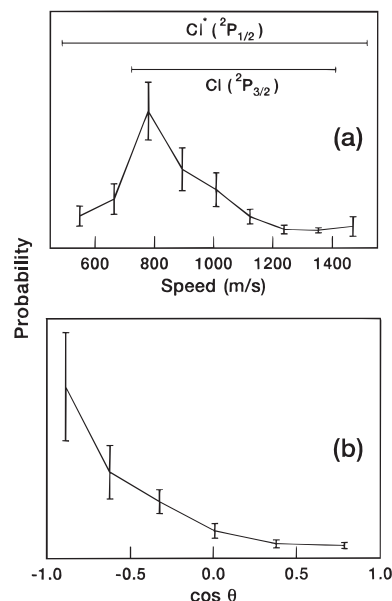


**Figure 4.** Product speed distribution and state-resolved differential cross section for DCI( $\nu=0, J=0$ ) from the reaction of Cl with ground-state CD<sub>4</sub>. Panel a shows the product speed distribution. The scale bars on the top show the laboratory-frame speed limits for both the reaction of spin-orbit excited (Cl <sup>2</sup>P<sub>1/2</sub>) and ground-state (Cl <sup>2</sup>P<sub>3/2</sub>) chlorine atoms. Panel b shows the state-resolved differential cross section inverted under the assumptions described in the text.

represents the time profile with  $\epsilon_{\text{ph}} \parallel \mathbf{Z}$ , and  $I_{\text{perp}}$  is recorded with  $\epsilon_{\text{ph}} \perp \mathbf{Z}$ . This summation removes the spatial anisotropy caused by polarized photolysis and allows for direct evaluation of the speed distribution.

These time profiles are converted to a speed distribution and then to a state-to-state differential cross section using methods described previously.<sup>4,5</sup> A small correction for flyout of fast products described previously<sup>4</sup> was again applied to the data. The basis set generation parameters were slightly adjusted to fit these data. Specifically, a larger transverse blurring was used than in our previous publication.<sup>4</sup> Steering error or jitter in steering or molecular beam velocity may cause the increased blurring. Our basis set checks did not uncover this effect because the products from this reaction move more slowly in the laboratory than even the slowest Cl atoms used for basis set checks described previously.<sup>4</sup> Additionally, the data were recorded at a lower extraction field (62 V/cm) than previous work, which is likely to increase the transverse blurring.

For Cl(<sup>2</sup>P<sub>3/2</sub>) + CD<sub>4</sub> at the present collisional energy, the center-of-mass frame moves at approximately 1070 m/s in the laboratory frame, and reactive products with no methyl excitation move at 350 m/s in the center-of-mass frame. At this collision energy, the reaction Cl(<sup>2</sup>P<sub>3/2</sub>) + CD<sub>4</sub> results in DCI between 700 and 1400 m/s. Spin-orbit excited Cl(<sup>2</sup>P<sub>1/2</sub>) (approximately 2% of the Cl<sub>2</sub> photolysis at this wavelength) also can react with CD<sub>4</sub> molecules. This reaction has a center-of-mass frame moving at 1010 m/s, and the reactive products can move up to 520 m/s in the center-of-mass frame. Therefore, the reaction Cl(<sup>2</sup>P<sub>1/2</sub>) + CD<sub>4</sub> results in DCI between 500 and 1500 m/s in the laboratory frame. We see evidence for both reactions in our data; therefore, the speed distribution was determined over the region 500–1500 m/s. Part of this evidence comes from measurement of the spatial anisotropy of the reactive product, which, in principle, can separate these two reactions. Deconvolution of the two reactions (Cl <sup>2</sup>P<sub>1/2</sub> and Cl <sup>2</sup>P<sub>3/2</sub>) is deferred to a future publication.

Figure 4a shows the speed distribution resulting from maximum-entropy analysis of the core-extracted time profile shown in Figure 3. The scale bars on the top of the plot show

the region of possible speeds for reaction with ground-state and spin-orbit excited Cl atoms (Cl( $^2P_{3/2}$ ) and Cl( $^2P_{1/2}$ ), respectively). Note that most of the product occurs in the region for the reaction of ground-state Cl( $^2P_{3/2}$ ) atoms; therefore, we make the qualitatively correct assumption that all the intensity in the region possible for the reaction of ground-state Cl( $^2P_{3/2}$ ) is caused by that reaction. The measurement of the reactive product spatial anisotropy also corroborates the validity of this assumption. For this paper, we use the DCI( $\nu=0, J=0$ ) speed distribution because it has little contribution from the reaction of Cl( $^2P_{1/2}$ ) + CD<sub>4</sub>. We compare this reaction [Cl( $^2P_{3/2}$ ) + CD<sub>4</sub>] to our previous results for the reaction of vibrationally excited methane because we observed no evidence of the reaction of spin-orbit excited Cl( $^2P_{1/2}$ ) atoms in those studies. Our present observation of the reaction of spin-orbit excited atoms is probably because our collision energy is so close to the barrier that the reaction of ground-state Cl( $^2P_{3/2}$ ) atoms is nearly closed. Presumably, the electronic energy available with the spin-orbit-excited Cl( $^2P_{1/2}$ ) atoms enhances the reaction.

The speed distribution peaks at the slowest possible speeds, which indicates the predominance of backscattering. We have inverted the speed distribution to a scattering distribution using the assumption of no methyl excitation and analyzing only the 700–1400 m/s region. Figure 4b shows the angular scattering distribution for the state-resolved reaction Cl( $^2P_{3/2}$ ) + CD<sub>4</sub> → DCI( $\nu=0, J=0$ ) + CD<sub>3</sub>. The differential cross section peaks at  $\cos \theta = -1$  and decays to half-maximum at  $\cos \theta = -0.65$ . The angular distribution is characteristic of a rebound mechanism in which the Cl atom reacts with the central C–H bond and the HCl product recoils in the backward direction in the center-of-mass frame.

#### 4. Discussion

Using the core-extraction technique, we have investigated the photoinitiated reaction of atomic chlorine with vibrationally unexcited methane. The product shows strong backscattering, and the product rotational-state distribution is very cold. In our previous investigation of the vibrationally excited reaction,<sup>5</sup> we found approximately 30% of the product is formed in HCl( $\nu=1, J$ ) with a cold rotational distribution; the remaining population is formed in HCl( $\nu=0, J$ ) and is more rotationally excited. The HCl( $\nu=1$ ) product is sharply forward scattered for low  $J$  and becomes nearly equally forward–backward scattered for high  $J$ ; the HCl( $\nu=0, J$ ) product is backward and side scattered. The behavior for HCl( $\nu=1, J$ ) agrees with the quasiclassical trajectory calculation of Wang *et al.*,<sup>9</sup> while the HCl( $\nu=0, J$ ) disagrees, as discussed later. Comparing the two reactions, we see that strong changes occur in both the state and scattering angle distributions upon vibrational excitation of the methane reagent. By means of these detailed observations, we have formulated how a chlorine atom abstracts hydrogen from methane and how vibrational excitation changes the abstraction. To generate a physical picture of the reaction, we use a simple correspondence between scattering angle and reactive impact parameter to show the distribution of impact parameters responsible for reaction. This scattering correlation is strictly true for hard spheres, but it is subsequently shown to be a good approximation for the Cl + CH<sub>4</sub> system.

**4.1. Relationship between Scattering Angle and Impact Parameter for Hard-Sphere Collisions.** For a hard-sphere interaction, the impact parameter determines the scattering angle. The impact parameter  $b$  is the distance of closest approach if the two reagents follow straight-line trajectories. Figure 5 shows the geometry of a collision between two hard spheres. For a given impact parameter, the tangent plane acts as a mirror,

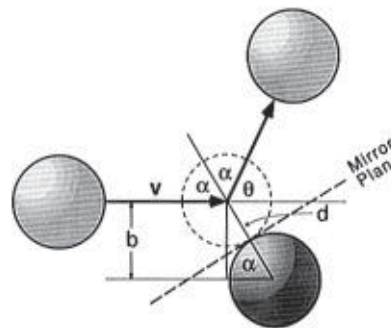


**Figure 5.** Relationship between scattering angle and impact parameter for hard-sphere collisions.

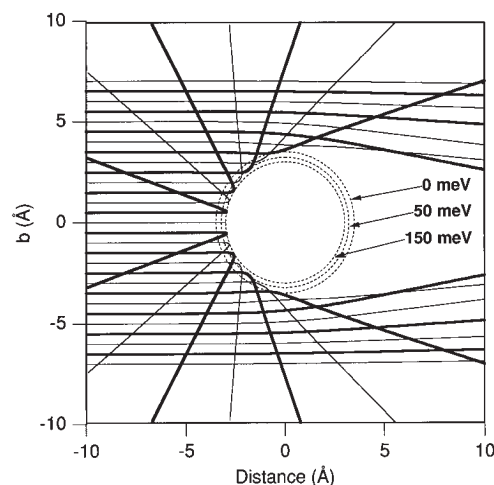


**Figure 6.** Classical elastic scattering trajectories of Cl atoms from the isotropic potential derived from molecular beam scattering measurements of Aquilanti *et al.*<sup>19</sup>

reflecting the product at twice the incident angle  $\alpha$ . The angle  $\alpha$  is given by trigonometry as  $\sin \alpha = b/d$ ; therefore, the cosine of the scattering angle  $\theta$  is

$$\begin{aligned} \cos \theta &= \cos(\pi - 2\alpha) = -\cos(2\alpha) \\ &= 2 \sin^2 \alpha - 1 \end{aligned} \quad (12)$$

Thus, for a hard sphere,

$$\cos \theta = 2b^2/d^2 - 1 \quad (13)$$

For reactive scattering, any significant lifetime to the transition state degrades the validity of this correlation. This lifetime effect is not problematic for Cl + CH<sub>4</sub> because the reaction is known to be direct. Similarly, attractive regions of the potential are possibly problematic. To investigate the effects of long-range attractive forces in the Cl–CH<sub>4</sub> system, we have run classical trajectory simulations to observe the degree of deflection of incoming trajectories under our reactive collision conditions (160 meV). The asymptotic interaction potential of chlorine with methane is known from molecular beam scattering data.<sup>19</sup> It shows a shallow van der Waals attractive well of 15 meV followed by the onset of a hard-sphere-like, steep repulsive wall at  $r = 3.5$  Å where  $r$  is the distance from the chlorine atom to the center of mass of the methane molecule. Although the potential is certainly incorrect for radii inside the hard-sphere potential (the potential does not allow for the chemical reaction we are observing), it represents a good picture for the deviations of reagents before collision. Assuming the product interaction is similar upon recoil, it also provides a picture of the exit well interaction. Figure 6 shows a set of elastic scattering trajectories of Cl atoms from methane molecules using the potential of

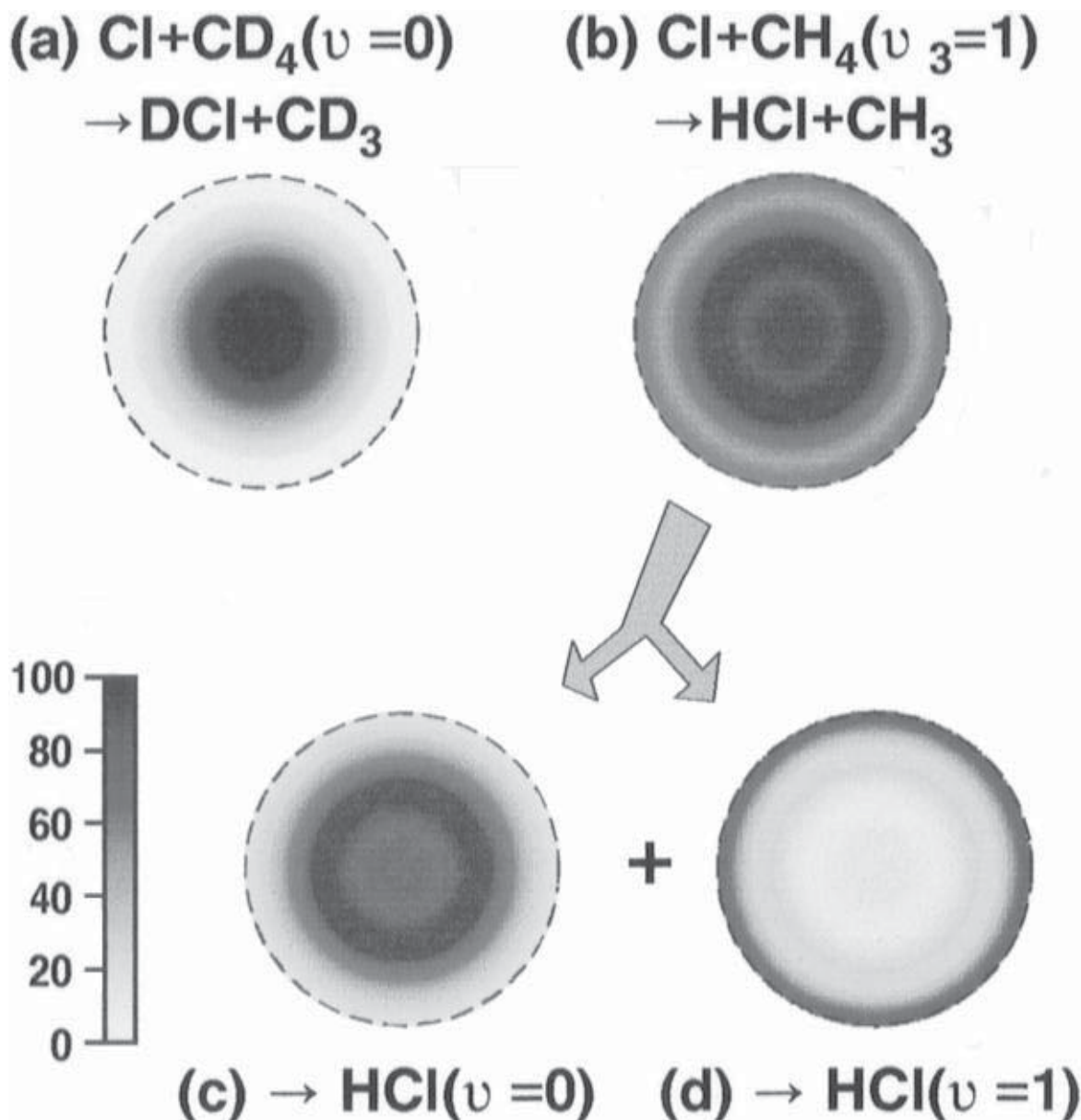


**Figure 7.** False-color reactive impact parameter distributions for the reaction of atomic chlorine with ground-state and vibrationally excited methane. In all panels, the dashed circle represents the maximal impact parameter for reaction assuming hard-sphere collisional dynamics. Therefore, the included area represents the hard-sphere collisional cross section. Panel a shows the  $b$  map for the DCI product from the reaction of Cl with ground-state CD<sub>4</sub>. Panel b shows the  $b$  map for the HCl product from the reaction of Cl with CH<sub>4</sub>( $v_3=1$ ). Panels c and d show the  $b$  map for the HCl( $v=0$ ) and HCl( $v=1$ ) products from the reaction of Cl with CH<sub>4</sub>( $v_3=1$ ). Summation of the data from panels c and d results in the data shown in panel b.

Aquilanti *et al.*<sup>19</sup> As would be expected for a collision with a translational energy more than 10 times larger than the van der Waals well depth, the scattering is very close to the hard-sphere prediction. All trajectories with an impact parameter less than the hard-sphere radius (3.5 Å) sample the repulsive wall of the potential, which causes a deflection at an angle within 18° of the hard-sphere prediction. The precollision deviation of the trajectory is insignificant, and the impact parameter represents the geometry at the beginning of the repulsive wall almost perfectly. In fact, the only significantly deviated trajectories are “near-miss” trajectories (approximately 4 Å impact parameter) that are precluded from reaction by the centrifugal barrier. Therefore, the reaction of atomic chlorine with methane is ideal for the purpose of obtaining the impact parameter directly from the scattering angle.

By using eq 13, we can convert the state-to-state differential cross sections into a picture of reactive impact parameters ( $b$  map). Figure 7a shows a false-color plot of the reactive impact parameters in the reaction Cl(<sup>2</sup>P<sub>3/2</sub>) + CD<sub>4</sub>. The dashed circle

represents the hard-sphere collisional cross section. Reaction occurs primarily during head-on collisions for the ground-state reaction, and little intensity appears on the periphery.

We can use the same procedure to create a picture of the vibrationally excited methane reaction. Figure 7b shows the analogous false-color plot of the reactive impact parameters in the reaction Cl + CH<sub>4</sub>( $v_3=1$ ). The plot shows the sum of both possible HCl product vibrational states. The vibrationally excited reaction shows a hard-sphere-like  $b$  map, with all impact parameters reacting with nearly equal efficiencies. The effect of vibrational excitation on the cone of acceptance of this reaction is visible as the differences between panels a and b. Figure 7c,d shows HCl vibrational-state-resolved false-color plots of the reactive impact parameters in the reaction Cl + CH<sub>4</sub>( $v_3=1$ ). Panel c shows the HCl( $v=0, J$ ) product, and panel d shows the HCl( $v=1, J$ ) product. Note that different impact parameter distributions contribute to the formation of HCl( $v=1, J$ ) and HCl( $v=0, J$ ) product from the reaction of atomic chlorine with vibrationally excited methane.

**4.2. Line-of-Centers Model.** Let us briefly review a simple model for the kinetic energy dependence of the collisional cross section. This model relates thermally averaged rate equation data to the highly nonthermal experiments described in this study. It also follows for prediction of the kinetic energy dependence of the reaction rate. The model is known as the line-of-centers model and is extensively described in the text of Levine and Bernstein.<sup>1</sup>

Consider a collision between two particles with a reduced mass of  $\mu$  at total energy  $E_T$ . During the collision, as the radial distance  $R$  decreases, the kinetic energy  $1/2\mu\dot{R}^2$ , which is initially completely translational, becomes converted to centrifugal energy  $E_T b^2/R^2$ , where  $b$  is again the impact parameter,

$$\begin{aligned} E_T &= T + V(R) \\ &= \frac{1}{2}\mu\dot{R}^2 + E_T \frac{b^2}{R^2} + V(R) \end{aligned} \quad (14)$$

or

$$E_T \left(1 - \frac{b^2}{R^2}\right) = \frac{1}{2}\mu\dot{R}^2 + V(R) \quad (15)$$

Thus, the approach motion of the two reagents is equivalent to that of a particle of mass  $\mu$  moving in a potential  $V(R)$  with an effective kinetic energy (the energy along the line of centers) equal to  $E_T(1 - b^2/R^2)$ —the larger the impact parameter, the smaller the effective kinetic energy. This effect is visible in Figure 6. The zero impact parameter trajectory penetrates the repulsive potential over the 150 meV contour [the reagent turns around when the collisional energy (160 meV) is completely converted to potential energy], while the 2.5 Å impact parameter trajectory penetrates only to approximately 50 meV.

For a reaction with an energy threshold, we must take into account both the centrifugal barrier and the threshold energy barrier,  $E_0$ . At some separation  $d$  the centrifugal barrier is  $E_T b^2/d^2$  so that

$$E_T \geq E_0 + E_T(b^2/d^2) \quad (16)$$

is the condition that the kinetic energy of motion along  $R$  evaluated at  $R = d$  is greater than or equal to the barrier to reaction.

We take  $b_{\max}$  to be the largest value of  $b$  for which this inequality is satisfied; therefore,  $b_{\max} = d(1 - E_0/E_T)^{1/2}$ . The reactive cross section is given by

$$\sigma_R = \int_0^\infty 2\pi b db P(b) \quad (17)$$

where  $P(b)$  is the probability of reaction as a function of impact parameter and the  $2\pi b db$  term is the volume element.  $P(b)$  is commonly known as the opacity function.

Consider the simple top-hat form of the opacity function where  $P(b)$  is a step function

$$P(b) = \begin{cases} p & b \leq b_{\max} \\ 0 & b > b_{\max} \end{cases} \quad (18)$$

The factor  $p$  (known as the steric factor) is included because not all collisions exceeding the barrier are in the correct configuration for reaction.

Integration of eq 17 using the top-hat form of the opacity function gives the reaction cross section

$$\sigma_R = p\pi d^2(1 - E_0/E_T) \quad \text{when } E_T > E_0 \quad (19)$$

The rate of reaction is the product of the cross section and the velocity. Because the experiments described here are monoenergetic, the observed rate is simply proportional to the cross section. The line-of-centers cross section form can be integrated with a thermal velocity distribution to arrive at an expression for the thermal rate constant:<sup>1</sup>

$$k_R = p\pi d^2 \langle v \rangle \exp\left(\frac{-E_0}{kT}\right) \quad (20)$$

where  $k$  is the Boltzmann constant and  $\langle v \rangle$  is the average relative velocity for the reagent at temperature  $T$ . Equation 20 is essentially the Arrhenius rate constant expression with the prefactor

$$A = p\pi d^2 \langle v \rangle \quad (21)$$

Using this formula, the steric factor can be derived from the experimentally determined Arrhenius prefactor. The observed activation energy is identified with the barrier to reaction; then eq 19 predicts the kinetic energy dependence of the reaction cross section. Equations 14–21 are well-known and presented elsewhere.<sup>1</sup> We restate them to provide the necessary background for using the line-of-centers model to predict the form of the differential cross section.

Using the hard-sphere relationship between the impact parameter and the scattering angle, we can predict the differential cross section. The differential form of the reaction cross section (eq 17) is

$$d\sigma_R/db = 2\pi b P(b) \quad (22)$$

To arrive at the center-of-mass differential cross section, we change  $db$  to  $d \cos \theta$  using the volume element obtained by differentiation of eq 13

$$\frac{db}{d \cos \theta} = \frac{d^2}{4b} \quad (23)$$

Therefore, the simple top-hat opacity function  $P(b)$  predicts the differential cross section to have the form

$$\frac{d\sigma_R}{d \cos \theta} = \begin{cases} 1/2 p\pi d^2 & -1 \leq \cos \theta < \cos \theta_{\max} \\ 0 & \cos \theta_{\max} < \cos \theta \leq 1 \end{cases} \quad (24)$$

where

$$\cos \theta_{\max} = 1 - 2E_0/E_T \quad (25)$$

Consequently, the line-of-centers model along with the hard-sphere relation between scattering angle and impact parameter makes the prediction that the reaction probability versus impact parameter is constant for all collisions with enough energy to surmount the energy threshold for reaction and the centrifugal barrier for a collision at that impact parameter. This behavior implies an angular scattering distribution that is constant between back scattering and a maximal scattering projection ( $\cos \theta_{\max}$ ) that depends on the reagent translational energy. Although this step function form is clearly not quantitatively realistic, this model predicts that the scattering has a cutoff given by eqs 24 and 25.

As Figure 4b shows, the ground-state reaction product intensity peaks at  $\cos \theta = -1$  with respect to the incoming

chlorine direction and decays to half maximal intensity at a projection of  $\cos \theta = -0.65$ . Using the preferred barrier height from the thermal rate data and the experimental collision energy, the line-of-centers model predicts a cutoff projection of  $\cos \theta_{\max} \approx -0.5$  for the Cl + CH<sub>4</sub> reaction. The kinetic isotope effect in this reaction should make this cutoff projection more negative for Cl + CD<sub>4</sub>. (Assuming the barrier has no zero-point energy for the transferring atom, the prediction is  $\cos \theta_{\max} \approx -0.8$ .) Compared to a real chemical reaction, the line-of-centers model is clearly naive, but its prediction of a cutoff angle that is qualitatively similar to the observed half-width indicates that the model offers a good simplified picture of the dynamics.

The angular scattering distributions are consistent with the predictions of a line-of-centers model for an activated process. Ultimately, however, the utility of any such theory is in its ability to predict reactivity. One prediction that can be checked experimentally is the effect of translational excitation of the reactants. The simple line-of-centers model predicts that the cone of acceptance opens with translational excitation. This opening should lead to a broader angular scattering distribution. Preliminary experiments appear to confirm this behavior for this reaction.

**4.3. Understanding Vibrational Enhancement.** Recent experimental and theoretical investigations have shown that, for reactions of diatomic molecules and small polyatomic molecules, reagent vibration dramatically changes chemical reactivity.<sup>1,3-5,17,18,20-29</sup> Understanding reagent vibrational excitation effects allows for control over chemical reactivity; it also reveals a more detailed picture of the motions responsible for reaction. Comparison of the vibrationally excited with the ground-state reaction results in a detailed view of the effects of vibrational excitation on this reaction. The present study represents a step toward a mechanistic understanding of the effect of vibrational excitation on a polyatomic chemical reaction; it leads to a model for one mechanism of mode-specific control of hydrogen abstraction reactions.

Much of the evidence for the conclusion that vibration alters reactivity is based on studies of reactions of atoms with diatomic molecules. Polanyi and co-workers<sup>17,18</sup> predicted that the location of the barrier to a chemical reaction relates to the relative efficacy of vibrational and translational energy in surmounting the barrier. Polanyi predicted that a reaction that has a late barrier (a barrier with a geometry more like the products than the reagents) should be enhanced by reagent vibrational energy more effectively than by translational energy. The vibration, by extending the reagent bond, effectively accesses a late barrier because the transition state resembles more closely the product; *i.e.*, it has a long reagent bond and short product bond. Thereby, observation of the effects of vibrational excitation probes features of the potential energy surface of the reaction (assuming that one potential energy surface is sufficient to describe the reaction dynamics).

In contrast to reactions of diatomic reagents, in which only one vibrational mode of the reagent participates, polyatomic reagents possess a number of different vibrational motions, and reactions of polyatomic reagents result in branching between possible reaction products. For several simple reactions, mode-specific chemistry (the dependence of branching into various open product channels on the reagent mode excited) has been observed.<sup>5,20-29</sup> The idea of understanding the nature of the transition-state region through observation of vibrational enhancement can be extended to polyatomic reactions through mode-specific chemistry. Thereby, mode-specific vibrational enhancement maps the reaction coordinate for formation of each product channel and increases understanding of the reaction mechanism.

In a straightforward example of mode-specific chemistry, excitation of either the O–H or O–D stretching in HOD enhances the probability of breaking the excited bond in reaction with hydrogen and chlorine atoms.<sup>20,21,23,25,29</sup> These observations indicate that O–H and O–D stretching are along the reaction coordinate for abstraction of the respective atom and that their barriers are late along the respective reaction coordinates. Sometimes, interpretation of the results of a mode-specific chemistry study may be more complex. For example, intramolecular vibrational redistribution and collision-induced mixing of vibrations during the time scale of the reaction can significantly cloud the window mode-specific chemistry opens for understanding polyatomic chemical reactions. These mode-mixing complications are interesting, however, as they affect the ability to control reactivity. They also signal the crossover between direct and statistical dynamics.

As evidenced by both the large changes in angular scattering behavior and rate enhancement caused by C–H stretching in methane, the dynamics of hydrogen abstraction from CH<sub>4</sub> are markedly affected by vibrational excitation. Significant rate enhancement caused by C–H stretching excitation was predicted in the *ab initio* study of Duncan and Truong.<sup>10</sup> The classical trajectory study of Wang *et al.*<sup>9</sup> did not investigate the reaction of ground-state methane. To understand the effects of vibrational excitation, we first draw conclusions from the thermal rate data on this reaction and then interpret our rotational-state distributions and reactive impact parameter distributions.

*Comparison with Thermal Rate Data.* Comparison of the Arrhenius preexponential factor to that predicted by a hard-sphere collisional cross section results in a steric factor, which provides a measure of the probability for a collision to have proper geometry for reaction.<sup>1</sup> Within the line-of-centers theory, eq 21 relates the Arrhenius prefactor to the steric factor  $p$  based on an assumed chemical interaction distance  $d$ . Molecular beam studies of the total scattering cross section of atomic chlorine by methane show the isotropic interaction to become repulsive at approximately 3.5 Å,<sup>19</sup> which provides one estimate for  $d$ . Another estimate for  $d$  is the chlorine-to-carbon distance in the transition-state region as found from *ab initio* quantum structure calculations of the Cl–H–CH<sub>3</sub> transition state. Both Truong *et al.*<sup>7</sup> and Dobbs and Dixon<sup>8</sup> calculate this distance to be approximately 2.8 Å. From eq 21 and with these two estimates of  $d$ , we obtain steric factors of 1/30 for the hard-sphere radius and 1/20 for the transition-state radius.<sup>30</sup> This small steric factor indicates that very few collisions are of the correct geometry to result in product formation.

Small Arrhenius prefactors seem to be a feature of the hydrogen abstraction reactions of O and Cl with hydrocarbons. Luntz and Andresen<sup>31</sup> noted this behavior in their studies of atomic oxygen (O <sup>3</sup>P) with hydrocarbons. They interpreted this behavior as an effect of a constrained linear transition state, in which hydrogen abstraction occurs only when the oxygen atom approaches within a tight cone surrounding the reacting C–H bond direction. Their experimental observation of cold rotational-state distributions<sup>31</sup> is consistent with a linear transition-state breakup in which little torque is applied to the forming OH radical. Quasi-classical trajectory simulations<sup>32</sup> of these reactions on model potential energy surfaces showed that product OH was backscattered, again in accord with a predominance of linear trajectories in chemically reactive collisions.

**4.4. Rotational-State Distributions.** Luntz and Andresen<sup>31,32</sup> argued for a correlation between the product rotational-state distribution and the collinearity of the transition state. Their argument is predicated on the assumption of an impulsive release as the mechanism of product rotational excitation. In the reaction of atomic chlorine with vibrationally excited methane,

we demonstrated that forward-scattered products do not follow this prediction because of breakdown of the assumptions of the model.<sup>3,5</sup> When the reaction product is backscattered, however, the atomic reagent is turned back toward its original direction by the chemical forces. This redirection (reverse thrust) requires an impulsive force to be active at the transition-state region. Therefore, the correlation of rotation with transition-state linearity should be more relevant for backscattered products. For  $\text{Cl} + \text{CD}_4$ , which results only in backscattered products, a bent C–D–Cl angle at the transition state produces rotation of the product by pushing on the D atom, which then orbits the Cl. A simple calculation shows transition-state bend angles less than  $5^\circ$  are consistent with  $J \leq 2$ .<sup>3</sup> Although such a tight cone of reaction about the C–D bond is probably quantitatively unrealistic, low rotational excitation does indicate a preference for a linear transition-state geometry.<sup>33</sup> Additionally, in the line-of-centers model, the steric factor  $p$  is the integral of the hard-sphere surface that results in chemical reaction. Therefore, a steric factor of 1/20 to 1/30 indicates that some amount less than 5% of the accessible hard-sphere surface is reactive. Thus, the steric factor is consistent with the observation of low rotational excitation and aids us in depicting the dynamics of the reaction.

We can also use this correlation of rotation with the constrained nature of the transition-state region for the reaction of vibrationally excited methane. For the  $\text{HCl}(v=0)$  products of the reaction with vibrationally excited methane, backscattering predominates and a relatively hotter rotational distribution was observed. This scattering result disagrees with the quasiclassical trajectory calculation of Wang *et al.*,<sup>9</sup> who predict that  $\text{HCl}(v=0, J)$  product is on average forward scattered. This disagreement may be a result of the potential energy surfaces used in their study, which were arranged to show peripheral dynamics of the  $\text{HCl}(v=1)$  product. Because the  $\text{HCl}(v=0)$  product is backward and side scattered, an impulsive release model allows qualitative inversion of the rotational distribution to predict a bending angle of the transition state. Previously, we found the vibrationally excited reaction produces a rotational distribution of  $\text{HCl}(v=0, J)$  that peaks at  $J = 3$  and 4, indicating a significantly more open bend-angle dependence to the barrier. These data imply that the vibrationally excited reaction has a less constrained transition-state structure.

**4.5. Reactive Impact Parameter Distributions.** The  $b$  map for the ground-state reaction (Figure 7a) is qualitatively similar to the prediction of the line-of-centers model. It peaks at zero impact parameter and decays rapidly as the impact parameter increases. The line-of-centers model predicts a cutoff (at  $b_{\text{max}}$ ) when the centrifugal barrier becomes high enough to prevent reaction, which is in qualitative agreement with Figure 7a. The  $b$  map for the vibrationally excited reaction (Figure 7b) shows hard-sphere-like scattering; collisions at any impact parameter inside the hard-sphere radius  $d$  react with nearly equal efficiency. This change implies that vibrational excitation lowers the requirement for line-of-centers energy, effectively eliminating the centrifugal barrier.

The line-of-centers model predicts a cross section at 0.16 eV collision energy of  $0.27p\pi d^2$  (this number assumes a barrier height of 2.7 kcal/mol) for the  $\text{Cl}(^2\text{P}_{3/2}) + \text{CH}_4$  reaction. If vibrational excitation were simply to remove the energy threshold for reaction (*i.e.*, lower  $E_0$  to 0) without changing the steric factor, the cross section would increase to  $p\pi d^2$ . This elimination of the activation energy is sufficient to fit the hard-sphere-like  $b$  map of the vibrationally excited reaction, yet the reaction cross section should be enhanced only by a factor of  $1/0.27 = 3.7$ . This prediction is significantly lower than the experimentally observed factor of 30. To explain this failure

of the line-of-centers model, we propose that more of the hard-sphere area of the vibrationally excited methane is reactive—the steric factor  $p$  is larger. This idea is supported by the observation of increased rotational excitation for the  $\text{HCl}(v=0)$  product of the vibrationally excited reaction. Similarly, a weaker requirement for linearity of the transition state should allow stripping to give  $\text{HCl}(v=1, \text{low } J)$  product scattered in the forward direction, as experimentally observed.

Therefore, we propose a mechanism for vibrational enhancement of the reaction cross section in which the excitation lowers the necessity for line-of-centers energy while it decreases the constraint for transition-state collinearity. This mechanism of vibrational enhancement is the origin of mode-specific chemistry previously found in the  $\text{Cl} + \text{CHD}_3(v_1=1)$  reaction, for which we observed preferential abstraction of the vibrationally excited hydrogen atom.<sup>5</sup> This study also indicates that reactive systems with significantly constrained transition-state structures (as evidenced by small Arrhenius  $A$  factors compared to gas-kinetic collisional rates) are good candidates for vibrational enhancement and possibly for mode-specific reaction control.

## 5. Summary

Pictures of the transition-state region for the reaction of chlorine with methane are observed through measurement of asymptotic scattering properties of the reaction. The weak interactions of reagents and products outside the chemically interesting part of the potential allow measurements of state-to-state scattering distributions to be mapped to specific collisional geometries. A simple line-of-centers model with a steric factor that describes the tightness of the transition state is used as a framework for picturing the reaction. The ground-state reaction is found to have an angular scattering distribution qualitatively similar to the prediction of this model. The rotational distribution for the ground-state reaction is extremely cold, which indicates a highly collinear interaction at the transition state. The necessity for collinearity is also suggested by the steric factor for the reaction obtained from application of the line-of-centers model to thermal rate data. Vibrational excitation radically changes the scattering distributions and product energy partitioning. This change is viewed as caused by both opening the cone of acceptance for the reaction by lowering the barrier to reaction and by lessening the necessity for C–H–Cl collinearity in the transition-state region.

## References and Notes

- (1) Levine, R. D.; Bernstein, R. B. *Molecular Reaction Dynamics and Chemical Reactivity*; Oxford University Press: New York, 1987.
- (2) Morrison, R. T.; Boyd, R. N. *Organic Chemistry*, 5th ed.; Allyn and Bacon: Boston, 1987.
- (3) Simpson, W. R.; Orr-Ewing, A. J.; Zare, R. N. *Chem. Phys. Lett.* **1993**, *212*, 163–171.
- (4) Simpson, W. R.; Orr-Ewing, A. J.; Kandel, S. A.; Rakitzis, T. P.; Zare, R. N. *J. Chem. Phys.* **1995**, *103*, 7299–7312.
- (5) Simpson, W. R.; Rakitzis, T. P.; Kandel, S. A.; Orr-Ewing, A. J.; Zare, R. N. *J. Chem. Phys.* **1995**, *103*, 7313–7335.
- (6) Atkinson, R.; Baulch, D. L.; Cox, R. A.; Hampson, R. F., Jr.; Kerr, J. A.; Troe, J. *J. Phys. Chem. Ref. Data* **1992**, *21*, 1125–1168.
- (7) Truong, T. N.; Truhlar, D. G.; Baldrige, K. K.; Gordon, M. S.; Steckler, R. *J. Chem. Phys.* **1989**, *90*, 7137–7142.
- (8) Dobbs, K. D.; Dixon, D. A. *J. Phys. Chem.* **1994**, *98*, 12584–12589.
- (9) Wang, X.; Ben-Nun, M.; Levine, R. D. *Chem. Phys.* **1995**, *197*, 1–17.
- (10) Duncan, W. T.; Truong, T. N., submitted.
- (11) Shafer, N. E.; Orr-Ewing, A. J.; Simpson, W. R.; Xu, H.; Zare, R. N. *Chem. Phys. Lett.* **1993**, *212*, 155–162.
- (12) Kinsey, J. L. *J. Chem. Phys.* **1977**, *66*, 2560.
- (13) Hall, G. E. In *Twelfth Combustion Research Conference*; The Combustion Research Facility of Sandia National Laboratory: Livermore, CA, 1990; p 122.

- (14) Aoiz, F. J.; Brouard, M.; Enriquez, P. A.; Sayos, R. *J. Chem. Soc., Faraday Trans.* **1993**, *89*, 1427–34.
- (15) Kim, H. L.; Wickramaaratchi, M. A.; Zheng, X.; Hall, G. E. *J. Chem. Phys.* **1994**, *101*, 2033–2050.
- (16) Shafer-Ray, N. E.; Orr-Ewing, A. J.; Zare, R. N. *J. Phys. Chem.* **1995**, *99*, 7591.
- (17) Polanyi, J. C.; Wong, W. H. *J. Chem. Phys.* **1969**, *51*, 1439.
- (18) Polanyi, J. C. *Acc. Chem. Res.* **1972**, *5*, 161.
- (19) Aquilanti, V.; Cappellitti, D.; Pirani, R. *J. Chem. Soc., Faraday Trans.* **1993**, *89*, 1467–1474.
- (20) Sinha, A.; Hsiao, M. C.; Crim, F. F. *J. Chem. Phys.* **1990**, *92*, 6333–4.
- (21) Sinha, A.; Hsiao, M. C.; Crim, F. F. *J. Chem. Phys.* **1991**, *94*, 4928–35.
- (22) Bronikowski, M. J.; Simpson, W. R.; Girard, B.; Zare, R. N. *J. Chem. Phys.* **1991**, *95*, 8647–8648.
- (23) Bronikowski, M. J.; Simpson, W. R.; Zare, R. N. *J. Phys. Chem.* **1992**, *97*, 2194–2203.
- (24) Bronikowski, M. J.; Simpson, W. R.; Zare, R. N. *J. Phys. Chem.* **1992**, *97*, 2204–2208.
- (25) Sinha, A.; Thoenke, J. D.; Crim, F. F. *J. Chem. Phys.* **1992**, *96*, 372–6.
- (26) Guettler, R. D.; Jones, G. C., Jr.; Posey, L. A.; Zare, R. N. *Science* **1994**, *266*, 259–261.
- (27) Chiu, Y.; Fu, H.; Huang, J.; Anderson, S. L. *J. Chem. Phys.* **1994**, *101*, 5410–5412.
- (28) Chiu, Y.; Fu, H.; Huang, J.; Anderson, S. L. *J. Chem. Phys.* **1995**, *102*, 1199–1216.
- (29) Metz, R. B.; Thoenke, J. D.; Pfeiffer, J. M.; Crim, F. F. *J. Chem. Phys.* **1993**, *99*, 1744–51.
- (30) The reaction of atomic chlorine with methane shows positive curvature in its Arrhenius plot (that is increased reactivity at high temperature compared to extrapolation of low-temperature data). This behavior leads to larger *A* factors and higher activation energies at high temperature. The use of a higher *A* factor would increase the steric factor reported here, but expressions employing a higher *A* factor also have a larger activation energy. Specifically, the high-temperature rate expression of Clyne and Walker (Clyne, M. A. A.; Walker, R. F. *J. Chem. Soc., Faraday Trans.* **1973**, *69*, 1547) includes a steric factor 5 times larger than used here, but it also predicts no reactivity at our collision energy because its barrier height is larger than the present study's collision energy. Therefore, we feel that the use of low-temperature *A* factors to predict the steric factor is reasonable in this study. It is interesting to note that in this study we find translational energy is less effective in promoting reaction than vibrational energy. Therefore, extrapolation of low-temperature data, where the translational barrier is primarily probed (because of low populations of vibrationally excited states of methane), should underestimate the high-temperature rate, for which both vibration and translation increase reactivity.
- (31) Andresen, P.; Luntz, A. C. *J. Chem. Phys.* **1980**, *72*, 5842–5850.
- (32) Luntz, A. C.; Andresen, P. *J. Chem. Phys.* **1980**, *71*, 5851–5856.
- (33) The reaction of atomic fluorine with methane also appears to show this behavior of low rotational excitation (see: Agrawalla, B. S.; Setser, D. W. In *Gas-Phase Chemiluminescence and Chemi-ionization*; Fontijn, A., Ed.; Elsevier Science Publishers, BV: Amsterdam, 1985; p 157).
- (34) van der Zande, W. J.; Zhang, R.; Zare, R. N.; McKendrick, K. G.; Valentini, J. J. *J. Phys. Chem.* **1991**, *95*, 8205–8207.

JP952627N